

## Eccentric Black Hole Mergers in Dense Star Clusters: The Role of Binary-Binary Encounters

MICHAEL ZEVIN,<sup>1,\*</sup> JOHAN SAMSING,<sup>2</sup> CARL RODRIGUEZ,<sup>3</sup> CARL-JOHAN HASTER,<sup>4,5</sup> AND ENRICO RAMIREZ-RUIZ<sup>6,7</sup>

<sup>1</sup>*Center for Interdisciplinary Exploration and Research in Astrophysics (CIERA) and Dept. of Physics and Astronomy, Northwestern University, 2145 Sheridan Road, Evanston, IL 60208, USA*

<sup>2</sup>*Department of Astrophysical Sciences, Princeton University, Peyton Hall, 4 Ivy Lane, Princeton, NJ 08544, USA*

<sup>3</sup>*Pappalardo Fellow; MIT-Kavli Institute for Astrophysics and Space Research, 77 Massachusetts Avenue, 37-664H, Cambridge, MA 02139, USA*

<sup>4</sup>*Canadian Institute for Theoretical Astrophysics, 60 St. George Street, Toronto, Ontario, M5S 3H8, Canada*

<sup>5</sup>*LIGO Laboratory and MIT-Kavli Institute for Astrophysics and Space Research, 77 Massachusetts Avenue, 37-664H, Cambridge, MA 02139, USA*

<sup>6</sup>*Department of Astronomy and Astrophysics, University of California, Santa Cruz, California 95064, USA*

<sup>7</sup>*Niels Bohr Institute, Blegdamsvej 17, 2100 København Ø, Denmark*

### ABSTRACT

We present the first systematic study of both binary-single and binary-binary black hole interactions with the inclusion of general relativity. By including general relativistic effects in the equations of motion during strong encounters, the dissipation of orbital energy from the emission of gravitational radiation can lead to inspirals and mergers with appreciable eccentricities when entering the sensitive frequency ranges of the LIGO and Virgo gravitational-wave detectors. It has been shown that binary-single interactions significantly contribute to the rate of eccentric mergers, but no studies have looked exclusively into the contribution from binary-binary interactions. To this end, we perform binary-binary and binary-single scattering experiments with general relativistic dynamics up through the 2.5 post-Newtonian order included, both in a controlled setting to gauge the importance of non-dissipative post-Newtonian terms and derive scaling relations for the cross-section of inspirals, as well as experiments tuned to the strong interactions from state-of-the-art globular cluster models to assess the relative importance of the binary-binary channel at producing inspirals and resultant eccentricity distributions. Although binary-binary interactions are 10–100 times less frequent in globular clusters than binary-single interactions, their longer lifetime and more complex dynamics leads to a higher probability for inspirals to occur during the encounter. We find that binary-binary interactions contribute 25–45% of the eccentric mergers which occur during strong black hole encounters in globular clusters, regardless of the properties of the cluster environment. The inclusion of higher multiplicity encounters in globular clusters therefore have major implications on the predicted rates of highly eccentric binaries potentially detectable by the LIGO/Virgo network. As gravitational waveforms of eccentric inspirals are distinct from those generated by merging binaries which have circularized, measurements of eccentricity in such systems would highly constrain their formation scenario.

*Keywords:* gravitational waves — black hole physics — globular clusters: general — methods:  $N$ -body simulations — stars: kinematics — binaries: close

### 1. INTRODUCTION

The multiple discoveries of coalescing binary black hole (BBH) systems by the advanced network of gravitational-wave (GW) interferometers (Abbott et al. 2016c,b,a, 2017a,b,c) has led to significant interest in the astrophysical mechanisms responsible for their formation and subsequent merger. One evolutionary channel that may significantly contribute to the population of BBHs is dynamical formation within dense stellar environments such as globular clusters (GCs) and

nuclear star clusters (NSCs) (Portegies Zwart & McMillan 2000; Downing et al. 2009, 2011; Rodriguez et al. 2015, 2016a). Through dynamical friction, black holes (BHs) tend to migrate towards the cores of clusters, where stellar densities can be over a million times higher than the stellar density of our solar neighborhood (Lightman & Shapiro 1978). In these tightly-packed collisional environments, BHs frequently interact with one another, swapping partners and hardening their orbits, thereby losing any memory of their primordial orbital states (e.g., McMillan et al. 1991; Hut et al. 1992; Fregeau & Rasio 2007). BBH mergers from dynamical environments thereby imprint unique and potentially

\* zevin@u.northwestern.edu

detectable characteristics in their GW waveforms relative to BBHs whose progenitors evolved in isolation, providing a possible route for discriminating between the various scenarios proposed for BBH formation.

In recent years, much attention has been focused on the BH spin orientations as a means to discriminate different BBH formation channels (Rodriguez et al. 2016b; Stevenson et al. 2017; Talbot & Thrane 2017; Vitale et al. 2017; Farr et al. 2017a,b; Gerosa et al. 2018; Sedda & Benacquista 2018; Schröder et al. 2018); BBHs that evolve in isolation are expected to have spin vectors that are relatively aligned with the angular momentum of the binary, whereas BBHs that assemble dynamically will have spin vectors distributed isotropically on the sphere. However, if the spin magnitudes of heavy black holes are naturally low, the ability to discern formation scenarios using spin parameters is stifled. Mass distributions may also have utility once dozens to hundreds of observations are made (Stevenson et al. 2015; Mandel et al. 2016; Zevin et al. 2017) or if second generation BH mergers are found with masses in the putative pair instability upper mass gap (O’Leary et al. 2016; Fishbach et al. 2017; Rodriguez et al. 2018a).

While our ability to measure the BBH spins may be stymied by low spin magnitudes, the orbital eccentricity of the binary is entirely a function of the well-understood dynamics that assembled the system. Eccentricity is often overlooked when discussing the parameters of merging BBHs; GW emission is highly efficient at circularizing the orbit of an inspiraling binary (Peters 1964) and most formation scenarios predict the binary to have evolved in isolation for substantial periods of time before merger, thereby circularizing its orbit to a point where any measurable semblance of eccentricity would be lost before entering the sensitive frequency band of ground-based GW detectors. Furthermore, matched-filtering searches for GWs do not utilize eccentric templates (Usman et al. 2016; Messick et al. 2017), necessitating methods of detection that are promising but significantly less effective than matched-filtering (Tai et al. 2014; Coughlin et al. 2015; Tiwari et al. 2016; Huerta et al. 2017; Gondán et al. 2017a,b; Huerta et al. 2018; Klein et al. 2018; Rebei et al. 2018; Gondán & Kocsis 2018). However, recent work modeling the strong binary-single encounters which harden BBHs in GCs find that resonating interactions (RIs) of BH systems (i.e., interactions of three or more bodies which evolve chaotically over many orbital times before reaching an endstate) can facilitate rapid and highly-eccentric mergers when post-Newtonian (pN) effects, particularly the emission of GWs, are included. (Gültekin et al. 2006; Samsing et al. 2014; Haster et al. 2016; Samsing & Ramirez-Ruiz 2017; Rodriguez et al. 2018a; Samsing 2018; Samsing et al. 2018). Traditionally, modeling of chaotic BH interactions have relied on Newtonian  $N$ -body simulations (e.g., Hut &

Bahcall 1983; Fregeau et al. 2004). Shown semi-analytically in Samsing et al. (2014, 2017a); Samsing (2018) and with full numerical simulations in Rodriguez et al. (2018a), the inclusion of pN terms in the  $N$ -body equations of motion are found to have a significant impact on the evolution and outcome of such encounters.

During resonating encounters, numerous meta-stable *intermediate-state* (IMS) binaries form before the interaction ceases through the ejection of enough components. These encounters can be long-lived, especially when the mass ratios are near unity and no component is preferentially ejected (Heggie 1975), therefore leading to dozens of IMSs during a single RI. Each IMS binary synthesized during the interaction will acquire an orbital eccentricity drawn from a quasi-thermal distribution. If an IMS binary has a high enough eccentricity (or, if two unbound compact objects pass close enough to one another during such an encounter), gravitational radiation will significantly dissipate orbital energy during periape passages, which can lead to a rapid GW inspiral (Quinlan & Shapiro 1987). Due to the swiftness of these inspiral timescales, the system will not have time to fully damp its orbital eccentricity, leading to appreciable eccentricities in the frequency ranges of ground-based GW interferometers such as Advanced LIGO (Aasi et al. 2015) and Advanced Virgo (Acernese et al. 2015) detectors with as many as  $\sim 5\%$  of these events having eccentricities greater than 0.1 at a GW frequency of 10 Hz (e.g. Samsing 2018; Rodriguez et al. 2018a).

Other formation scenarios which may facilitate BBH inspirals with eccentricities accessible by current ground-based GW detectors have also been identified, including hyperbolic encounters between BHs in nuclear clusters (O’leary et al. 2009; Kocsis & Levin 2012) and through the evolution of hierarchical triples (e.g., Antonini & Perets 2012; Antonini et al. 2016; Silsbee & Tremaine 2017; Antonini et al. 2017; Rodriguez & Antonini 2018; Hoang et al. 2017; Randall & Xianyu 2018b,a; Hamers et al. 2018; Liu & Lai 2018), particularly when non-secular evolution is properly considered (Antonini et al. 2014). Motivated by formation scenarios with this highly discriminating characteristic, efforts have been made to quantify the measurability of eccentric signals, and have placed limits on the amount of eccentricity needed in a signal to distinguish it from circular. For example, Lower et al. (2018) finds that eccentricities will be discernible for a signal analogous to GW150914 detected by the Advanced LIGO/Virgo network if the eccentricity is  $\gtrsim 0.05$  at a GW frequency of 10 Hz.

Recent work modeling BH encounters in GCs with pN dynamics have focused on binary-single BH encounters. In this paper, we present the first systematic study of binary-binary BH scattering encounters with pN terms up to and including the 2.5pN order. In addition to gauging the dependence of

the inspiral cross-section on initial conditions of the binary-binary configuration, we use binary-single and binary-binary interactions from state-of-the-art cluster models to compare the efficiency and relative rate of inspirals from these two types of encounters. We find that, while binary-single encounters are more than an order of magnitude more prevalent in cluster environments, binary-binary encounters are naturally more efficient at inducing GW inspirals during the encounter; in total binary-binary interactions contribute 25–45% of eccentric in-cluster mergers, irrespective of the cluster properties. Similar to binary-single interactions in GCs, BBH mergers from binary-binary encounters lead to three distinct populations of eccentric GW inspirals (Rodriguez et al. 2018a; Samsing & D’Orazio 2018). Though only the most rapidly inspiraling population has eccentricities accessible by ground-based GW detectors, eccentricity measurements of the other two populations will be attainable by future space-based interferometers such as LISA (Samsing & D’Orazio 2018; D’Orazio & Samsing 2018).

We first outline the numerical methods and pN additions to the  $N$ -body equations of motion in Section 2. In Section 3, we discuss the dependence of various endstates, including GW inspirals, on the initial properties of the binary-binary system. We also, for the first time, quantify how non-dissipative pN terms affect the inspiral probability in such encounters. Following this, we investigate the relative efficiency of binary-binary encounters compared to their binary-single counterparts from state-of-the-art cluster models and examine the eccentricity distribution of inspirals from binary-binary encounters. We discuss the implications of our findings and future work in Section 4, and summarize our main conclusions in Section 5.

## 2. NUMERICAL METHODS

Orbital dynamics involving more than two bodies is chaotic; no general analytic solution can be derived and subtle changes in the initial conditions of the system can lead to vastly different outcomes (Samsing & Ilan 2018). Therefore, it is common to perform a large number of scattering experiments that span the possible initial configurations to quantitatively determine how variations in initial conditions probabilistically affect interaction outcomes. (Heggie 1975; Hut & Bahcall 1983; Fregeau et al. 2004; Antognini & Thompson 2016). In particular, three-body binary-single scatterings have been extensively studied (e.g., Fregeau et al. 2004), and more recently this problem has been reexamined with the inclusion of GW dissipation in the equations of motion (Samsing et al. 2014). The problem of 4-body binary-binary scattering has been investigated to a lesser extent, as the multitude of possible endstate configurations and necessary computational requirements make higher multiplicity encounters much more complicated to examine with

scattering experiments. However, cluster modeling predicts that a significant number binary-binary BH encounters do occur in the cluster cores (Antonini et al. 2016), and such encounters are vital for the formation of triple systems as the Newtonian energetics of 3-body encounters in GCs will typically not allow for the formation of a bound triple.

In investigating the impact of such encounters, studies such as Fregeau et al. (2004) and later Antognini & Thompson (2016) performed detailed scattering experiments for binary-binary interactions (as well as those for other higher-multiplicity systems in Antognini & Thompson 2016) in the Newtonian regime to comprehensively gauge how variations in initial conditions affect endstate cross-sections. However, as these studies did not specifically target encounters of compact objects or take into account pN effects, there have been no studies which investigate the role binary-binary encounters involving BH systems in the strong gravity regime, and how such interactions instigate GW inspirals.

In this study, we Monte Carlo sample over the pre-encounter extrinsic parameters of binary-binary systems, and evolve  $O(10^5)$  scatterings for each set of initial conditions to determine cross-sections of particular endstates, as well as properties of the subsequent binary inspirals.

### 2.1. Initial conditions & pre-encounter setup

Each system is defined by its component masses, semi-major axis (SMA) and eccentricity prior to interaction, and the relative incoming velocity of the two pre-encounter binaries. Masses and orbital parameters are notated by subscripts in a top-down fashion as in Fregeau et al. (2004), where leftmost indices in the subscripts denote the separate binary systems prior to interaction and rightmost indices the components of the binary. For example,  $m_{12}$  indicates the secondary component of the target binary and  $a_2$  the SMA of the incoming binary. We sample the location of the orbit by solving Kepler’s equations numerically and sampling the mean anomaly, and randomly sample the three orientation angles of each binary:  $\phi_{\text{peri}} = [0, 2\pi]$ ,  $\cos(\theta_i) = [-1, 1]$ ,  $\phi_{\text{ascn}} = [0, 2\pi]$  where  $\phi_{\text{peri}}$  is the angle of periape,  $\theta_i$  is the inclination, and  $\phi_{\text{ascn}}$  is the angle of ascending node.

Given an incoming velocity at infinity  $v_\infty$ , we define our maximum impact parameter similar to Hut & Bahcall (1983)<sup>1</sup>:

$$b_{\text{max}} = \left( \frac{4v_{\text{crit}}}{v_\infty} + 3 \right) a_{\text{max}} \quad (1)$$

where  $v_{\text{crit}}$  is the critical velocity at which the total energy of the system is zero,  $v_\infty$  is the typical incoming velocity at

<sup>1</sup> The maximum sampled impact parameter is only used for gridded scattering experiments; for encounters that we extract from cluster models the true impact parameter is recorded and used.

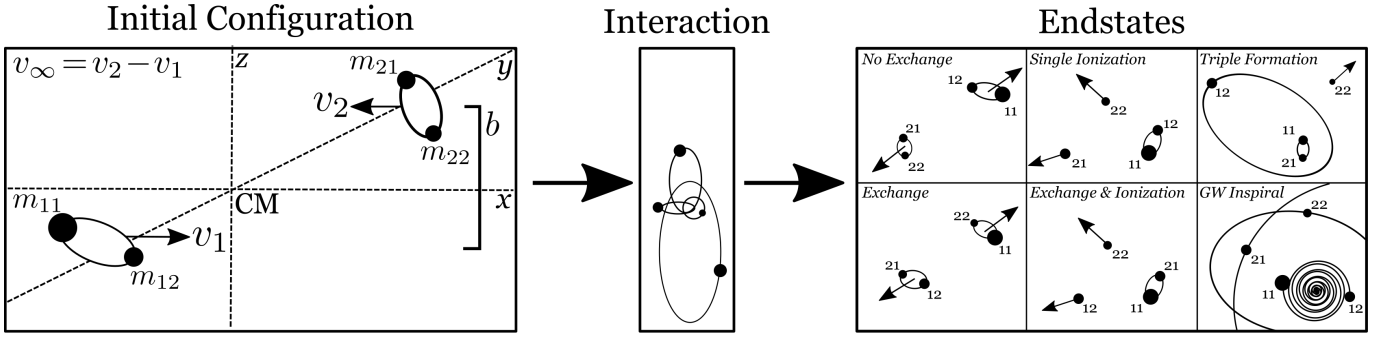


**Figure 1.** Schematic of initial configuration, resonant interaction, and potential endstates of a pN binary-binary BH encounter.

infinity, and  $a_{\max}$  is the largest of the two binary SMAs. We then draw the impact parameter of the incoming system at infinity  $b_{\infty}$  uniformly from a circle of radius  $b_{\max}$ . To limit integration time at large separations, we analytically evolve the incoming system forward from  $b_{\max}$  and  $v_{\infty}$  using conservation of energy and angular momentum until one of the two binary systems reaches a threshold point of  $F_{\text{tid}}/F_{\text{rel}} = 10^{-5}$ , where  $F_{\text{tid}}$  is the tidal force on the components of one binary from the other binary and  $F_{\text{rel}}$  is the gravitational force between two components within a single binary. We then integrate the pN equations of motion until a physical or computational endstate is reached using the  $N$ -body integration scheme detailed in [Samsing et al. \(2017b\)](#). As we only consider the scattering of systems composed entirely of black holes, finite-size effects such as tides are ignored.

## 2.2. Quantifying interaction probability

To quantify the probability of a particular outcome, we define a cross-section of interaction in the standard way:

$$\sigma_X = \pi b^2 \frac{N_X}{N_{\text{tot}}} \quad (2)$$

where  $N_X$  is the number of realizations that result in endstate  $X$  for a given initial condition and  $N_{\text{tot}}$  is the total number of realizations run for a particular initial condition. From this, the rate for a particular outcome is approximated as  $\Gamma_X \simeq n_{\text{BBH}} \sigma_X v_{\text{disp}}$  where  $v_{\text{disp}}$  is the velocity dispersion and  $n_{\text{BBH}}$  is the number density of BBHs in the cluster core. For investigating the relative rate of a particular outcome it is useful to normalize the cross-section by the sum of the areas of the two interacting binaries, a quantity referred to as the reduced cross-section:

$$\hat{\sigma}_X = \frac{b^2}{a_1^2 + a_2^2} \frac{N_X}{N_{\text{tot}}}. \quad (3)$$

There are two types of uncertainty to consider in our scattering experiments. The first is statistical uncertainty due to the finite number of scattering experiments, which is simply a Poisson counting uncertainty:

$$\Sigma_{X,\text{stat}} = \frac{\sigma_X}{\sqrt{N_X}}. \quad (4)$$

The second source of uncertainty is due to computational constraints; certain interactions will form long-lived metastable states or be thrown into wide orbits, which take an exceedingly long time to integrate. We mark systems as *unresolved* if they integrate for more than  $10^4$  times the average initial orbital time of the two incoming binaries or if the computing time of the integration exceeds 1 hour. Such unresolved systems result in a systematic uncertainty:

$$\Sigma_{X,\text{sys}} = \pi b_{\max}^2 \frac{N_{\text{unres}}}{N_{\text{tot}}}, \quad (5)$$

which only acts to increase the cross-section uncertainty.

We typically find  $\lesssim 5\%$  of systems for a particular initial configuration are unresolved due to completing  $\geq 10^4$  orbits without reaching an endstate. However, this outcome still dominates over low-probability endstates such as inspirals. Throughout this text, our upper error bars show only statistical uncertainty for readability. We find this to be reasonable, as it is expected that if fully integrated the endstates for unresolved systems will proportionally follow the endstates of resolved systems. However, we still include the cross-sections of unresolved systems, which if added to the cross-section of another endstate will provide a highly conservative upper limit. We stress again that this uncertainty can only act to *increase* the cross-section of resolved endstates.

## 2.3. Halting criteria and possible outcomes

Binary-binary scattering experiments lead to various potential outcomes, which we refer to as *endstates*. We define similar endstates to those in [Antognini & Thompson \(2016\)](#), with the addition of the crucial “inspiral” endstate which becomes relevant when pN effects are considered (see [Figure 1](#) for schematics of possible endstates). In all the endstates, we define an object as “unbound” when it has positive energy relative to all other components, is moving away from center of mass of the interaction, and its tidal force on other components in the interaction is less than  $10^{-3}$  times their relative binding force. We classify possible outcomes as follows:

- **NO EXCHANGE:** Two bound binaries unbound from one another, with constituent components that are

identical to the initial configuration. This can either result from a weak interaction fly-by or a RI that leads to a final configuration identical to the initial configuration.

- **EXCHANGE:** Two bound binaries unbound from one another, with constituent components that are different from the initial configuration.
- **SINGLE IONIZATION:** One bound binary which maintained its initial configuration and ionized the two components of the other binary.
- **EXCHANGE & IONIZATION:** One bound binary composed of two components that originated in different binaries, with the two remaining components ionized.
- **TRIPLE FORMATION:** One of the four components is ionized and a stable hierarchical triple is formed. We determine if a triple is stable according to the stability criterion from [Mardling & Aarseth \(2001\)](#):

$$\frac{a_1(1-e_1)}{a_{11}} > 2.8 \left[ \left( 1 + \frac{m_{11}}{m_{12}} \right) \frac{1+e_1}{\sqrt{1-e_1}} \right]^{2/5} \left( 1 - \frac{0.3i}{\pi} \right) \quad (6)$$

where we again use the top-down notation in [Fregeau et al. \(2004\)](#) ( $a_{11}$  is the SMA of the inner binary in the triple,  $m_{12}$  is the total mass of the inner binary,  $m_{11}$  is the mass of the tertiary, etc.) and  $i$  is the inclination of the outer component's orbit relative to the orbital plane of the inner binary. Systems that reach this stable endstate can be examined further through secular evolution.

- **INSPIRAL:** Emission of GWs lead to a rapid inspiral and merger of two component black holes during the RI ([Samsing et al. 2014](#)). To avoid the breakdown of our numerical integration schemes as the two quasi-point particles come near contact, we determine this endstate when two particles are in a bound orbit ( $E_{ij} < 0$ ) and their SMA reaches a nominal value, namely  $a_{ij}/(R_{s,i} + R_{s,j}) < 10$ , where  $R_s$  is the Schwarzschild radius. Systems meeting this criterion will merge on a rapid timescale and perturbations from other component black holes in the RI can be neglected; for example, the orbit of two  $20 M_\odot$  black holes on a circular orbit at this limit will merge in less than three seconds.

Two additional endstates are possible: a full ionization (i.e., all components of the two binary systems become ionized) and a direct collision. However, these endstates are exceedingly rare relative to the other endstates; since  $v_\infty \ll v_{\text{crit}}$  for most cluster binaries fully ionizing encounters are energetically improbable, and the physical sizes of stellar mass black holes make direct collisions in unbound systems highly unlikely.

#### 2.4. Post-Newtonian equations of motion

The encounters we focus on in this study lead to relativistic velocities and interactions in the strong-field gravity regime; purely Newtonian dynamics fails to capture the true evolution. Though there is no general analytic expression for the equations of motion of relativistic bodies, pN theory approximates relativistic effects by formulating the equations of motion in increasing orders of  $(v/c)^\gamma$ . The 2.5pN order, which includes terms in the pN expansion with  $\gamma = 5$ , is the lowest pN order at which the dissipative energy effects of GW emission are introduced. Prior studies which focused on binary-single BH encounters found the inclusion of GW emission can lead to rapid GW captures and inspirals (e.g., [Samsing et al. 2014](#)).

In this study, we include pN terms in the equations of motion up to and including the 2.5pN term (see e.g. [Blanchet 2014](#)). Though the 2.5pN term is the primary driver facilitating rapid and eccentric mergers during RIs, the 1pN and 2pN terms, which govern periaapse precession, may play an important role in the evolution of strong-field 4-body encounters. Furthermore, precession of the orbit can suppress the highly-eccentric oscillations in hierarchical triples that lead to mergers with measurable eccentricities ([Blaes et al. 2002](#)). To ensure the correct implementation of pN terms, we evolve a single BBH system to verify that the evolution of SMA, eccentricity, and angle of periaapse match analytical expectations ([Peters 1964](#)), and find that the orbit-averaged pN energy is conserved when only pN terms below the 2.5 order are included in the equations of motion ([Mora & Will 2004](#)).

### 3. SCATTERING EXPERIMENTS

With our endstates defined and pN equations of motions implemented, we performed  $\mathcal{O}(10^5)$  scatterings for each initial condition, specified by component masses, incoming velocity, orbital SMA, and orbital eccentricity. We Monte Carlo sample over all other extrinsic parameters defining the initial configuration of the system, accumulating statistics on various endstates and the orbital characteristics of resultant binaries.

First, we perform binary-binary scatterings in the strong encounter regime on a fixed grid with only one parameter of the system configuration varied. Next, we consider binary-binary and binary-single encounters from the classical channel of dynamical BBH formation: BBH assembly in old, metal-poor GCs. We use a few dozen GC models with various masses, metallicities, and virial radii generated using the Cluster Monte Carlo (CMC) code ([Joshi et al. 2000](#); [Chatterjee et al. 2010](#); [Morscher et al. 2013](#); [Rodriguez et al. 2016a](#)). Models are taken from [Rodriguez & Loeb \(2018\)](#) and [Rodriguez et al. \(2018b\)](#), with updates which include orbital dissipation from GWs and 2.5pN terms when integrating strong encounters ([Rodriguez et al. 2018a](#)). The initial

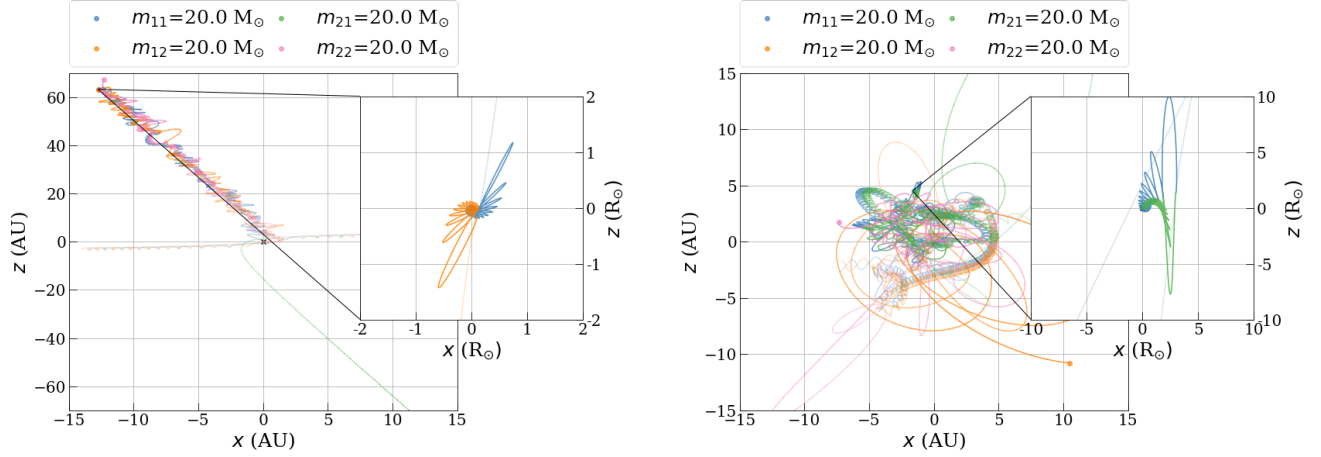


**Figure 2.** Example evolution of binary-binary BH encounters that lead to a GW inspiral. All components are  $20 M_{\odot}$ , initial binary SMAs are 1 AU, and  $v_{\infty}/v_{\text{crit}} = 0.01$ . Insets zoom into the highly eccentric inspiral. Trajectories are shaded to indicate the passage of time; darker shades correspond to later in the resonant interaction. The encounter on the left takes place over approximately 14 years and the encounter on the right over approximately 25 years. Animations for these interactions, as well as for other binary-binary interactions from this study, can be found at [https://michaelzevin.github.io/media/bbh\\_progenitors/](https://michaelzevin.github.io/media/bbh_progenitors/).

conditions of encounters used in our scattering experiments, as well as the relative abundance of binary-binary and binary-single interactions, are taken from these models. We analyze interactions from each cluster model separately to examine general trends in encounters as a function of cluster property.

### 3.1. Fiducial strong encounters

In the following two sections, we explore how the probability of inducing a GW inspiral is affected by the initial conditions of the interacting system using fiducial binary parameters, and quantitatively examine how non-dissipative pN terms influence this probability.

#### 3.1.1. Dependence on binary parameters

Figure 3 shows the scaling of endstate cross-sections as a function of SMA and SMA ratio,  $\alpha = a_2/a_1$ . Though incoming velocities also affect endstate probability, the velocity dispersion within the cores of GCs are typically low compared to the critical velocity of the binaries. To this end, we examine a grid of binaries with equal mass ratios in the hard binary limit ( $v_{\infty} \ll v_{\text{crit}}$ ), with fiducial values of  $v_{\infty}/v_{\text{crit}} = 0.01$  and component BH masses of  $m_{ij} = 20M_{\odot}$ .

We find the expected scaling relations derived for binary-binary encounters in the Newtonian regime (cf. Figure 3 in Antognini & Thompson 2016). The INSPIRAL endstate, which was not included in Newtonian scattering experiments, reaches a peak probability at  $\alpha \lesssim 1$  and occurs at a probability approximately two orders of magnitude less than the most probable endstate at equal SMA ratio (NO EXCHANGE). For values of  $\alpha \gg 1$  or  $\alpha \ll 1$ , we find that the INSPIRAL endstate probability once again drops; this is due to the tighter binary effectively acting as a single particle during the interaction, and the encounter proceeds similar to a 3-body interaction.

This will cause shorter-lived RIs with less IMSs than a typical 4-body encounter, thereby decreasing the probability of the INSPIRAL endstate.

Notably, the INSPIRAL endstate occurs at a higher probability for values of  $\alpha < 1$  compared to large values of  $\alpha$ , whereas the Newtonian endstates are all symmetric about  $\alpha$ . The bottom panel of Figure 3 shows the reason for this effect. We define the inspiral probability simply as

$$\mathcal{P}_{\text{insp},j} = \frac{N_{\text{insp},j}}{N_{\text{total},j}} \quad (7)$$

where  $N_{\text{total},j}$  is the total number of either binary-binary ( $j=\text{bb}$ ) or binary-single ( $j=\text{bs}$ ) scattering experiments that are performed and  $N_{\text{insp},j}$  is the number those encounters which lead to an INSPIRAL endstate. Thus, the reduced cross-section for an inspiral is given by

$$\hat{\sigma}_{\text{insp},j} = \mathcal{P}_{\text{insp},j} \hat{\sigma}_{\text{CI}} \simeq \mathcal{P}_{\text{insp},j} \frac{3GM}{a_0 v_{\infty}^2} \quad (8)$$

where  $M$  is the total mass of the 4-body system,  $a_0$  is the initial SMA of the target binary, and  $\sigma_{\text{CI}}$  is the cross-section for a close interaction where a system passes within a sphere of influence marked by the target binary's separation (Samsing et al. 2014).

For an IMS binary to undergo an inspiral during the RI its pericenter distance must be below some characteristic capture distance  $r_{\text{cap}}$ . The value of this distance is determined from where the GW energy loss integrated over one pericenter passage,  $\Delta E_p(r_p) \approx (85\pi/12)G^{7/2}c^{-5}m^{9/2}r_p^{-7/2}$  (see Hansen 1972), is comparable to the total energy of the few-body system (Samsing et al. 2017a,b) that in the hard binary limit is approximately the binding energy of the initial binaries,  $E_B(a_0) \propto m^2/a_0$  (see Samsing et al. 2014). Solving for

the pericenter distance at which  $\Delta E_p(r_{\text{cap}}) = E_B(a_0)$ , one now finds  $r_{\text{cap}} \propto m^{5/7} a_0^{2/7}$  (Samsing et al. 2017b). Since the eccentricity of the IMS binary follows a thermal distribution, the probability for a GW capture and inspiral is  $P_{\text{insp}} \propto r_{\text{cap}}/a_0$ . Thus, the reduced cross-section for an inspiral endstate scales as

$$\hat{\sigma}_{\text{insp},j} = \mathcal{P}_{\text{insp},j} \hat{\sigma}_{\text{CI}} \propto \frac{m^{12/7}}{a_0^{12/7} v_\infty^2} \propto \left(\frac{m}{a_0}\right)^{5/7} \quad (9)$$

where the last proportionality holds for our scattering experiments where the incoming velocity is fixed relative to the critical velocity of the target binary, which scales as  $v_{\text{crit}} \propto \sqrt{m/a_0}$ . For fixed  $v_\infty/v_{\text{crit}}$ , the reduced cross-section is directly proportional to the inspiral probability.

This scaling is consistent between binary-binary and binary-single encounters, as can be seen in the bottom panel of Figure 3. Though only shown for binaries which an SMA ratio of  $\alpha = 1$ , additional scattering experiments with SMA ratios of  $\alpha = 0.1$  and  $\alpha = 0.5$  found this scaling to be true regardless of the SMA ratio — the scaling of the INSPIRAL endstate probability as a function of SMA in the bottom plot is therefore true for each SMA ratio in the top plot. The peak in the inspiral probability for values of  $0.3 \lesssim \alpha \lesssim 0.8$  is due to the interplay of the two effect described above: though the inspiral probability increases as the SMA decreases, if  $\alpha$  becomes too small the tighter binary will act as a single particle and the interaction will effectively proceed as a 3-body encounter. Most importantly, though, is that we find the probability of a binary-binary encounter leading to a GW inspiral is 3–4 times higher than the probability of a binary-single encounter leading to a GW inspiral for any initial value of the SMA.

### 3.1.2. Effect of non-dissipative pN terms

We also examine how the inclusion of the 1pN and 2pN terms in the equations of motion affect the induction of inspirals during RIs. The reduced cross-section for the INSPIRAL endstate including (not including) the 1pN and 2pN terms can be seen in Figure 3 with filled (unfilled) blue circles. We find no measurable difference in the INSPIRAL cross-section when 1pN and 2pN terms are included compared to simulations where only the 2.5pN term is included. Though the statistical and systematic uncertainty affect our measurement of the INSPIRAL cross-section to a higher degree, our experiments show that the amplification or suppression of inspirals during RIs due to the inclusion of non-dissipative pN terms is limited to percent-level deviations at most. However, it is important to note that the 1pN and 2pN terms are crucial for following the evolution of encounters which result stable triples. Though we do not examine the evolution of such systems here, we refer the reader to Antonini et al. (2016).

### 3.2. Strong encounters in GCs

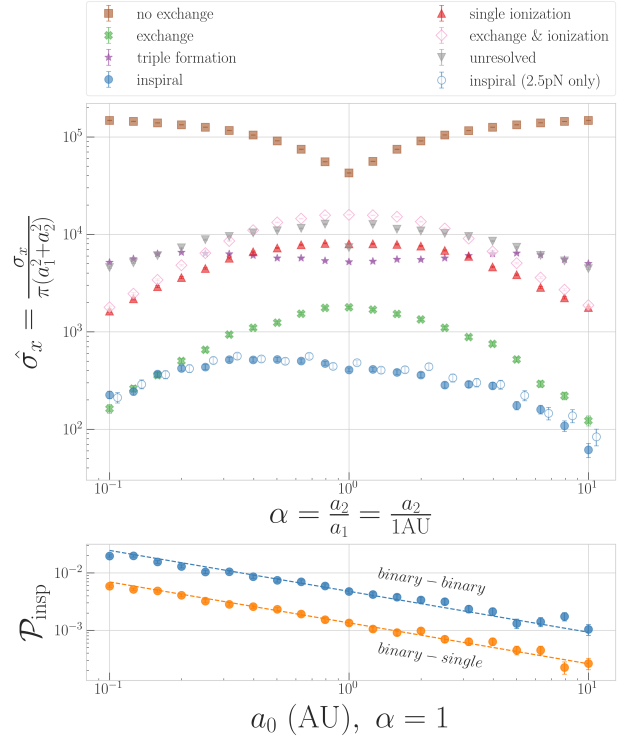


**Figure 3.** Reduced cross-sections for binary-binary endstates as a function of SMA ratio  $\alpha$  (top panel) and inspiral probability for binary-binary and binary-single inspirals as a function of SMA (bottom panel) in the hard binary limit. Since reduced cross-sections are normalized by the orbital area, the scaling relations are identical to those for a particular endstate probability. All systems have component masses of  $m=20 M_\odot$  and incoming velocities of  $v_\infty/v_{\text{crit}} = 0.01$ , with impact parameters sampled according to Equation 1. Top panel: the target binary has a fixed SMA of  $a_1 = 1\text{AU}$ . We find that the SINGLE IONIZATION and EXCHANGE endstates scale as  $\alpha^{-1}$  and  $\alpha^{-2}$ , respectively, as found in Antognini & Thompson (2016). For the INSPIRAL endstate, we show cross-sections for simulations where we include all pN terms up through the 2.5pN order (filled circles) and only include the 2.5pN order (open circles, artificially offset for readability); we find no statistically significant effect from the inclusion of lower-order non-dissipative pN terms. Bottom panel: SMAs are varied between  $10^{-1}$  and  $10^1$  AU, with a SMA ratio of unity. The reduced cross-sections of the INSPIRAL endstate scales as  $a^{-5/7}$ , similar to binary-single encounters (cf. Samsing et al. 2014).

We next perform binary-single and binary-binary BH scattering experiments informed from GC models, which provide a distribution of pre-encounter orbital parameters that is more representative of the systems in the universe. In particular, we gauge the relative contributions of binary-binary and binary-single encounters in inducing GW inspirals. Regardless of cluster properties, binary-single BH encounters occur  $\sim 10$ – $100$  times more frequently than binary-binary BH encounters. However, as seen in Figure 3, the probability of

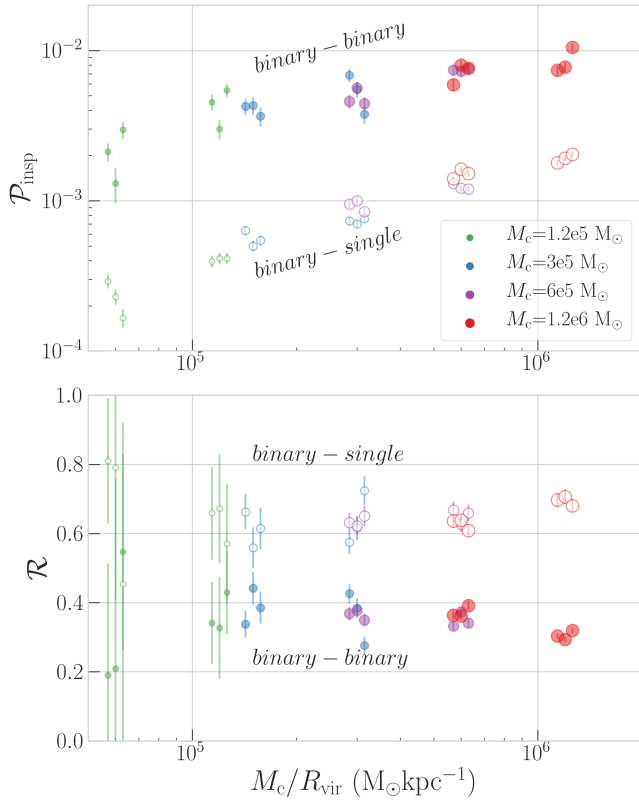


**Figure 4.** Inspiral probability (top panel, Equation 7) and inspiral contribution (bottom panel, Equation 10) for binary-binary (filled circles) and binary-single (open circles) encounters in GCs with varying masses, virial radii, and metallicities. Cluster models with different masses are differentiated by colored circles of different sizes. For each cluster compactness, we artificially offset clusters with different metallicity for readability; for each compactness value the leftmost point is for a metallicity of  $Z = 0.0005$ , the middle point for  $Z = 0.001$ , and the right point for  $Z = 0.005$ . We take into account statistical uncertainty on both  $\mathcal{P}_{\text{insp},j}^c$  and  $N_j^c$ .

the INSPIRAL endstate is higher in binary-binary encounters by a factor of  $\sim 3$ – $4$ . For our scattering experiments involving cluster binaries, we only include the  $2.5\text{pN}$  term, as the orbital characteristics are more accurately extracted and, as shown in Section 3.1.2, non-dissipative pN terms have a negligible effect on the cross-section of GW inspirals.

### 3.2.1. Inspiral efficiency of binary-binary interactions

In the top panel of Figure 4, we show the inspiral probability for binary-binary and binary-single encounters in a range of cluster models with various masses, metallicities, and virial radii. The cluster compactness is the dominant influence on inspiral probability, with metallicity playing no noticeable role; we therefore plot  $\mathcal{P}_{\text{insp}}$  for the various cluster models as a function of compactness, defined as  $M_c/R_{\text{vir}}$ , where  $M_c$  is the initial GC mass and  $R_{\text{vir}}$  its initial virial radius. Similar to our gridded scattering experiments, we find

the probability of inducing an inspiral from a binary-binary interaction is  $\sim 3$ – $4$  larger than that for a binary-single encounter.

We can define the contribution of binary-single or binary-binary inspirals to the total number of inspirals for a given cluster model as

$$\mathcal{R}_j^c = \frac{\mathcal{P}_{\text{insp},j}^c N_j^c}{\sum_k \mathcal{P}_{\text{insp},k}^c N_k^c} \quad (10)$$

where  $\mathcal{P}_{\text{insp},j}^c$  is the inspiral probability and  $N_j^c$  is the total number of binary-single ( $j=\text{bs}$ ) or binary-binary ( $j=\text{bb}$ ) interactions in a given cluster model. We find binary-binary inspiral contribution values of  $\mathcal{R}_{\text{bb}}^c \sim 25$ – $45\%$  for the GC models examined, with a median of  $36\%$ . The properties of the GC environment have little effect on  $\mathcal{R}_{\text{bb}}^c$ .

Analytical arguments in Samsing (2018) predict that the inspiral probability scales linearly with the cluster compactness. We see this linear trend for GC models with low compactness, though the inspiral probability flattens at high compactness values. This may indicate a critical compactness for which inspiral probability maximizes; we comment on this further in Section 4.

### 3.2.2. Eccentricity of inspirals

One of the most notable properties of GW inspirals from dynamical encounters is their eccentricity. We divide the BBH mergers from such encounters into 3 categories:

- **EJECTED INSPIRALS** are binary systems whose post-encounter center of mass velocity exceeds the escape velocity of the GC,<sup>2</sup> and evolve in isolation following their ejection. We only include systems that merge within a Hubble time in this population. As these systems merge over timescales ranging from tens of millions to billions of years, they have mostly circularized by the time GW emission evolves their orbits into the LIGO/Virgo sensitive frequency range, regardless of their post-encounter eccentricity.
- **IN-CLUSTER BINARY INSPIRALS** leave a resonating encounter in a hardened binary system with post-encounter velocities that do not exceed the escape speed of the cluster. If the SMA is small enough and/or the eccentricity is large enough, these binaries can merge through GW emission before encountering another object in the cluster. The typical interaction

<sup>2</sup> The escape velocity of a GC can change drastically as the cluster evolves over cosmic time. For each interaction in the GC models, the escape velocity from the location of the interaction at the time of the interaction is recorded, and this is compared to the post-encounter center of mass velocity to deem whether the system is ejected from the cluster.



timescale of objects in the core of a cluster is dependent on cluster properties and the age of the cluster. However, we can approximate the typical interaction timescale of a binary from its cross-section, which is dependent on the component masses and SMA of the binary. Taking a fiducial interaction timescale of  $\tau = 10$  Myr for a post-encounter binary with  $m_1 = m_2 = 20 M_\odot$  and  $a = 0.3$  AU (see [Samsing 2018](#)), and noting that the binary-single interaction cross-section is given by  $\sigma_{\text{bs}} = 6\pi Gma/v_{\text{disp}}^2$  where  $v_{\text{disp}}$  is the velocity dispersion, the typical time between binary-single interactions scales as

$$\tau_{\text{int}} \approx \frac{1}{n_{\text{BH}}\sigma_{\text{bs}}v_{\text{disp}}} \propto \frac{v_{\text{disp}}}{n_{\text{BH}}ma} \quad (11)$$

where  $n_{\text{BH}}$  is the number density of single black holes. We scale the fiducial value of  $\tau_{\text{int}}$  by the total mass and SMA accordingly for each post-encounter binary and compare it to the GW merger timescale:

$$\tau_{\text{insp}}(a_0, e_0) = \frac{12 c_0^4}{19 \beta} \int_0^{e_0} \frac{e^{29/19} [1 + (121/304)e^2]^{1181/2299}}{(1-e^2)^{3/2}} de, \quad (12)$$

where  $\beta$  is a constant factor dependent on the component masses and  $c_0$  is determined by the initial conditions  $a = a_0$  and  $e = e_0$ . If  $\tau_{\text{insp}} < \tau_{\text{int}}$ , the binary merges prior to its next encounter in the cluster and is therefore classified as an IN-CLUSTER BINARY INSPIRAL. Since these tight binaries merge on a shorter timescale than ejected binaries, they typically merge with eccentricities higher than those of ejected mergers.

- **GW CAPTURES<sup>3</sup>** are systems which inspiral and merge during the resonant encounter itself, and are determined when an INSPIRAL endstate is reached (see Section 2.3), or if a binary inspirals and merges within  $10^5$  seconds of its final encounter in the RI.<sup>4</sup> This can occur in the formation of a hard eccentric IMS binary which merges during the chaotic encounter, or through a highly eccentric capture where the two objects emit enough gravitational radiation during a close pass on a hyperbolic orbit for the binary to become bound and rapidly inspiral. This mechanism can even cause highly eccentric binaries to be formed

<sup>3</sup> In recent work, this category of GW inspirals is often referred to as THREE-BODY MERGERS. However, as a significant fraction of such mergers come from encounters featuring more than three bodies, we use the nomenclature GW CAPTURES in this text.

<sup>4</sup> We include this criterion because oftentimes the final interaction of the RI, which would eventually leave the binary in isolation, induces the highly-eccentric inspiral shortly after the isolation tidal threshold is reached and the system is marked as an ionization endstate.

within the sensitive frequency ranges of ground-based detectors, resulting in initial eccentricities close to unity and mergers which typically occur in less than a second after the system becomes bound.

We record the eccentricities and SMAs of each bound binary once an endstate is reached in our scattering simulations. To find the eccentricity at a particular GW frequency, we numerically solve for the orbital properties of the binary at a given eccentric peak frequency as in [Wen \(2003\)](#):

$$a(e) = \frac{1}{1-e^2} \left[ \frac{GM}{\pi} \frac{(1+e)^{1.1954}}{f_{\text{GW}}} \right]^{2/3}, \quad (13)$$

which is coupled to the differential equation from [Peters \(1964\)](#)

$$\left\langle \frac{da}{de} \right\rangle = \frac{12 a}{19 e} \frac{[1 + (73/24)e^2 + (37/96)e^4]}{(1-e^2)[1 + (121/304)e^2]}. \quad (14)$$

For cases where the binary forms at frequencies above  $f_{\text{GW}}$ ,  $e(f_{\text{GW}}) > 1$  and these equations are not differentiable. To distinguish these systems, we calculate the pericenter distance at a reference eccentricity of  $(1-e_{\text{ref}}) = 10^{-3}$ , where the pericenter distance is given by

$$R_p = (1-e)a(e) = (1-e) \frac{c_0 e^{12/19}}{(1-e^2)} \left[ 1 + \frac{121}{304} e^2 \right]^{870/2299} \quad (15)$$

where the constant  $c_0$  is determined by the orbital parameters recorded at the end of the integration ([Peters 1964](#)). We compare this distance to the SMA of the binary if it were on a circular orbit at an orbital frequency of  $f_{\text{orb}} = f_{\text{GW}}/2$ :

$$a_{\text{circ}} = \frac{GM}{\pi^2 f_{\text{GW}}^2}. \quad (16)$$

If  $R_p < a_{\text{circ}}$ , then the binary formed at a frequency greater than  $f_{\text{GW}}$ , and it is assigned an extremal eccentricity of  $e = 1$ . Since the  $R_p$  asymptotically approaches the true initial pericenter distance as  $e$  approaches 1, our choice of reference eccentricity has little effect on this procedure.

Similar to [Samsing & Ramirez-Ruiz \(2017\)](#) and [Rodriguez et al. \(2018a\)](#), we find GW inspirals induced from pN binary-binary RIs to have a distinctive imprint on the distribution of binary eccentricities. Figure 5 shows the eccentricity distributions for these three categories of dynamically-induced inspirals from binary-binary encounters. We find little difference in the shape of the binary-binary and binary-single eccentricity distributions in our simulations, and the highly eccentric peak in our binary-binary distributions is consistent with previous work ([Samsing & Ramirez-Ruiz 2017](#); [Rodriguez et al. 2018a](#)).

We also calculate the inspiral time ( $\tau_{\text{insp}}$ ) from the formation of the binary until the merger as in Equation 12. However, since we record the binary information at the point

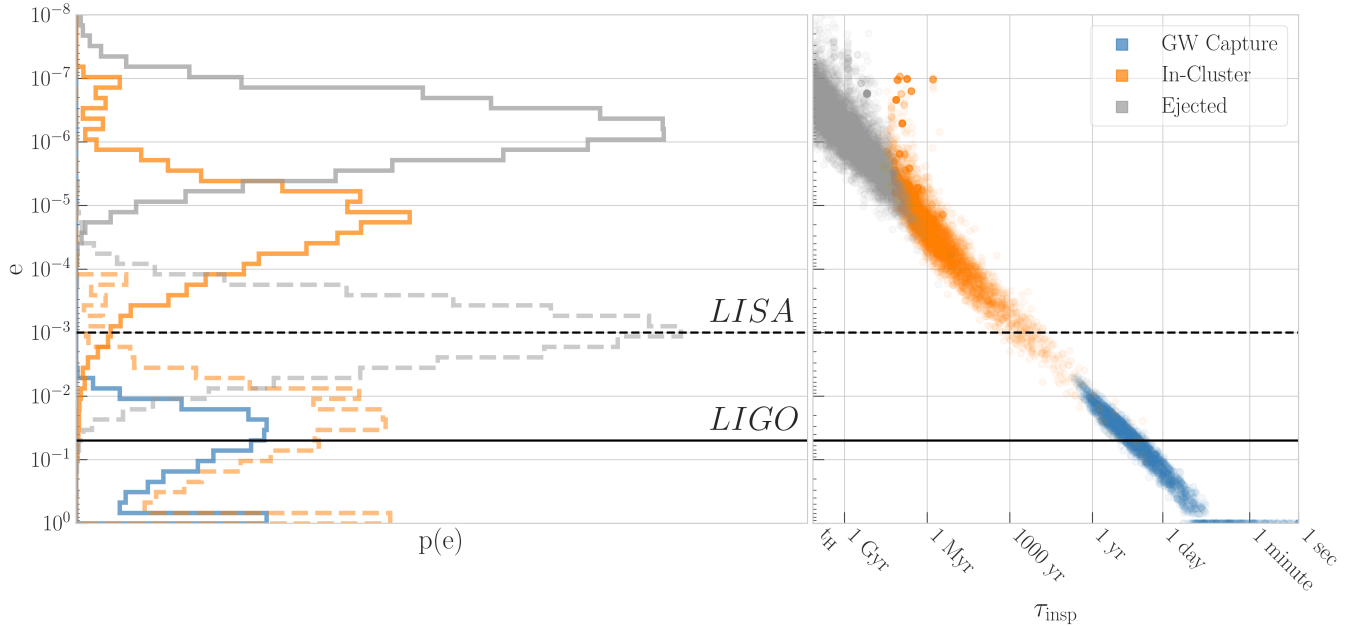


**Figure 5.** Eccentricity distributions and delay times resultant from three different populations of binary-binary induced inspirals: EJECTED INSPIRALS (gray), IN-CLUSTER BINARY INSPIRALS (orange), and GW CAPTURES (blue). Solid colored lines show the eccentricity at 10 Hz — the lower end of the LIGO/Virgo sensitive frequency range. Dashed colored lines show the eccentricity at  $10^{-2}$  Hz — the most sensitive frequency predicted for the space-based LISA detector. The solid and dashed black lines show minimum measurable eccentricities predicted for LIGO/Virgo (Lower et al. 2018) and LISA (Nishizawa et al. 2016), respectively. None of the GW captures are accessible by LISA, as they form at orbital frequencies above LISA’s sensitive frequency range.

when the simulations terminate, the orbital properties at binary formation for systems which reached an INSPIRAL end-state are ambiguous. To estimate the inspiral times of this population, we note that these systems are generally formed from highly eccentric captures, and therefore choose a high reference eccentricity of  $(1 - e_{\text{ref}}) = 10^{-3}$  at formation and calculate  $a_{\text{ref}}$  and  $\tau_{\text{insp}}$  accordingly.

The inspiral times for our three populations of GW inspirals can be seen in the right panel of Figure 5. The continuum of inspiral times between low-eccentricity GW CAPTURES and high-eccentricity IN-CLUSTER BINARY INSPIRALS supports our choice for  $e_{\text{ref}}$ . Additionally, we find that the inspiral times of GW CAPTURES are relatively insensitive to our choice of  $e_{\text{ref}}$ . We comment on this further, as well as other methods which have been utilized for calculating the inspiral times of GW CAPTURES in Section 4.

#### 4. DISCUSSION

Until recently, the prospect of detecting eccentric BH mergers with ground-based GW detectors was stifled by assumed long inspiral times and the ensuing damping of orbital eccentricities. However, the past couple years have shown substantial progress in identifying formation scenarios that can maintain appreciable eccentricity even at the high GW frequencies accessible to ground-based detectors, such as the merger of binaries in hierarchical triples from the Lidov-Kozai mechanism (Antonini et al. 2016; Silsbee & Tremaine

2017; Randall & Xianyu 2018a), single-single captures in NSCs (O’leary et al. 2009; Lee et al. 2010; Kocsis & Levin 2012), and RIs in the cores of stellar clusters (Rodriguez et al. 2018a; Samsing 2018). These channels all predict astrophysical rates within the predicted detection capabilities of the Advanced LIGO/Virgo network at design sensitivity (Abadie et al. 2010), and may be the most important feature in a GW waveform for definitively distinguishing its BBH progenitor from an isolated binary formation scenario. Prior to this study, the role binary-binary encounters in inducing eccentric GW inspirals was never systematically explored.

##### 4.1. Orbital properties following strong encounters

The black holes residing in the collapsed cores of GCs are susceptible to many strong encounters during their lifetimes, thereby erasing information about their primordial orbital histories. It is through these strong encounters that binary orbits tighten, as components eject from the interaction siphon orbital energy during their ionization. The distribution of binary orbital properties resulting from strong encounters is thereby largely independent of the properties of primordial binaries, but influenced by the initial energetics of the systems that take part in the strong encounter.

In the case of strong binary-single interactions, the average change in SMA between the incoming and outgoing binary can be analytically approximated using three-body energetics. From the normalized orbital energy distribution

for binary systems that are assembled in three-body processes (Heggie 1975), one finds that the mean fractional decrease in binary SMA from a strong binary-single encounter is  $\langle \delta_3 \rangle \approx 7/9$  (Samsing 2018).

In the four-body problem, strong encounters which go through a RI typically lead to two ejected and unbound components, requiring approximately double the orbital energy to be transferred to the kinetic energy of the ionized particles. Furthermore, the greater number of component BHs and larger mass in the interaction means the system's gravitational potential is slightly deeper, and ionization necessitates larger energy requirements. Therefore, one would expect the mean fractional decrease in SMA from a strong binary-binary encounter ( $\langle \delta_4 \rangle$ ) to be smaller, making the hardening process more drastic in binary-binary encounters.

Given two incoming binary BHs in the hard binary limit ( $v_\infty \ll v_{\text{crit}}$ ), the initial energy of the system is determined by the binding energy of the two binaries. Assuming equal masses and SMAs, this is given by

$$E_0 = -\frac{Gm^2}{a_0}. \quad (17)$$

If one of the two binaries becomes dissociated from the encounter and its components ejected, the maximum binding energy that the remaining binary could have is half of the initial energy of the encounter, and therefore

$$\delta_{4,\text{max}} = 0.5. \quad (18)$$

However, the ionized particles are typically ejected at speeds greater than the escape velocity. We estimate the typical ejection velocity from a strong encounter through conservation of energy in a binary-single encounter:

$$-\frac{Gm^2}{2a_0} = -\frac{Gm^2}{2\langle \delta_3 \rangle a_0} + \frac{1}{2}\mu_3 v_{\text{ion}}^2 \quad (19)$$

where  $\mu_3$  is the reduced mass of the 3-body system ( $2m/3$  for equal mass) and  $v_{\text{ion}}$  is the typical velocity of the ionized particle. Solving for  $v_{\text{ion}}$  yields

$$v_{\text{ion}} = \sqrt{\frac{3Gm}{2\langle \delta_3 \rangle a_0} (1 - \langle \delta_3 \rangle)}. \quad (20)$$

If we assume that the velocity of the ionized particles after the encounter is similar for binary-binary interactions, equating initial and final energy of an ionizing binary-binary interaction gives us

$$-\frac{Gm^2}{a_0} = -\frac{Gm^2}{2\langle \delta_4 \rangle a_0} + \frac{1}{2}(\mu_3 + \mu_4)v_{\text{ion}}^2 \quad (21)$$

where  $\mu_4$  is the reduced mass of the three-body metastable system and the ionized particle ( $3m/4$  for equal mass). Substituting  $v_{\text{ion}}$  from Equation 20 and solving for  $\langle \delta_4 \rangle$ , we get

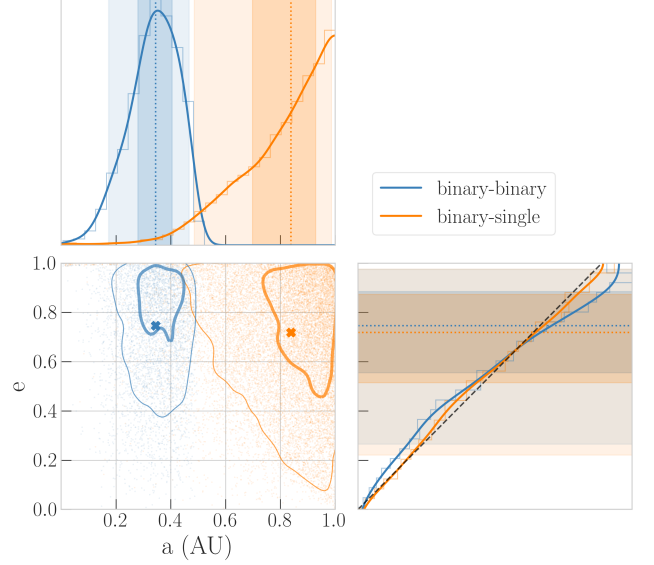


**Figure 6.** Post-encounter orbital properties for bound binaries following binary-binary (blue) and binary-single (orange) EXCHANGE & IONIZATION encounters, for fiducial encounters of systems initially on circular orbits with  $20 M_\odot$  component BHs, 1 AU initial orbital separation, and  $v_\infty/v_{\text{crit}} = 0.01$ . In the joint (marginal) distribution, the marker (dotted line), thick line (dark band), and thin line (light band) represent the median, 50%, and 90% credible regions. A thermal distribution is plotted over the marginal eccentricity distribution with a dashed black line. The typical post-encounter SMA for strong binary-binary interactions is clearly separable from the post-encounter SMA of binary-single interactions.

$$\langle \delta_4 \rangle = \frac{24\langle \delta_3 \rangle}{51 - 3\langle \delta_3 \rangle}. \quad (22)$$

If we assume a binary-single encounter does not harden the resultant binary at all,  $\langle \delta_3 \rangle = 1$  and  $\langle \delta_4 \rangle$  reduces its maximum value of  $\delta_{4,\text{max}} = 0.5$ . Using instead a value of  $\langle \delta_3 \rangle \approx 7/9$  as derived in Samsing (2018), we find a value of  $\langle \delta_4 \rangle \approx 0.38$  where again  $\langle \delta_4 \rangle$  is the mean fractional change in the SMA of the remaining binary after an ionizing 4-body encounter. Alternatively, one could instead assume the ejection process results from two successive ejections by the remaining binary which each have an equal effect on the hardening process. In this case,  $\langle \delta_4 \rangle$  is simply found to be  $0.5 \times \langle \delta_3 \rangle^2 = 0.30$ .

These analytical approximation are supported by the scattering experiments shown in Figure 6. Here, we plot the post-interaction orbital properties of bound binaries that underwent a binary-binary (blue) and binary-single (orange) EXCHANGE & IONIZATION.<sup>5</sup> As expected, the bound post-

<sup>5</sup> We focus on the EXCHANGE & IONIZATION endstate because this guarantees the binary-single system went through a strong encounter. Since we only track the resultant particle configurations, if the output configuration is identical to the input configuration it is ambiguous whether a resonating encounter and ionization occurred or simply a weak fly-by.

interaction binary eccentricities follow a thermal distribution. For the post-interaction SMAs, we find median and 90% credible values of  $0.84^{+0.12}_{-0.21}$  and  $0.34^{+0.09}_{-0.10}$  for  $\langle\delta_3\rangle$  and  $\langle\delta_4\rangle$ , respectively, consistent with our analytical approximations. Although our simple estimates seem to provide a good understanding of the expected hardening of the remaining binary after a strong binary-binary encounter, we refer the reader to [Leigh et al. \(2016\)](#) and [Leigh et al. \(2017\)](#) for a more detailed study of the problem.

#### 4.2. *Inspirational contribution from binary-binary encounters*

The literature on pN scattering experiments has thus far focused on the contribution of binary-single encounters as the main driver of GW inspirals in GCs. By performing scattering experiments initialized on binary-single and binary-binary encounters extracted from cluster models, we were able to quantify the importance of binary-binary encounters in the pN scenario for the first time. Even though binary-binary encounters have a larger interaction cross-section, the relative scarcity of binary BH systems compared to isolated BHs in cluster cores lead to these interactions occurring an order of magnitude less often than binary-single BH interactions. However, binary-binary interactions lead to more complex RIs that last significantly longer than their binary-single counterparts, facilitating 3–4 times more metastable IMS binaries before the system dissociates. Since the probability of generating a GW capture and inspiral scales linearly with the number of IMSs, this causes binary-binary encounters to be  $\sim 3$ –4 times more likely to induce a highly-eccentric inspirals. This culminates in a 25–45% amplification in the rate of GW captures predicted solely from binary-single interactions ([Samsing 2018](#)). The relative rate of GW captures in GCs is therefore expected to be  $\sim 10\%$  with approximately half of these mergers having eccentricities large enough to be measurable by LIGO/Virgo. These numbers have also been found using pure numerical techniques ([Rodriguez et al. 2018a](#)); the remarkable consistency between these different approaches indicates the robustness of this result.

Importantly, we find that the relative contribution between binary-binary and binary-single encounters is insensitive to properties of the cluster environment, such as cluster mass, compactness, and metallicity. This indicates that these numbers are a good measure of the binary-binary inspiral contribution in the true, astrophysical GC population. However, one interesting property of GC models that was not investigated in this study was the initial binary fraction. Our models use an initial binary fraction of 5%, which is loosely based on the observed binary fraction of Milky Way GCs ([Rubenstein & Bailyn 1997](#); [Bellazzini et al. 2002](#); [Ivanova et al. 2005](#)). Though this may be representative of the initial binary fraction for low-mass stars, it is not necessarily the case for high-mass stars which are the progenitors of BHs. The high-mass

binary fraction is much more opaque, as progenitor stars of high-mass primordial binaries finished their stellar evolution early in the history of the cluster and are no longer observable in the local universe. An increase in the high-mass primordial binary fraction may lead to more BH mergers prior to mass segregation, however it is unlikely to alter the contribution of binary-binary BH interactions in the cluster core since the primordial orbital properties of the segregated BH sub-population are erased from dynamical interactions.

Another way in which binary-binary interactions may lead to more in-cluster mergers is through triple formation. In the Newtonian regime, a binary-single encounter will not be able to synthesize a bound, stable triple system. Though energy losses through GW emission can theoretically lead to a bound triple from a strong binary-single BH interaction, the presence of an extra component in the interaction makes binary-binary encounters much more efficient at generating bound triple systems ([Fregeau et al. 2004](#); [Antognini & Thompson 2016](#)), as the ejection of the fourth BH can efficiently drain energy from the encounter and result in a bound, stable 3-body state (see the triple cross-section in Figure 3). If the Lidov-Kozai oscillation timescale is significantly shorter than the periape-precession timescale, the third body can induce a highly-eccentric mergers in the inner binary before the outer binary of the triple is disrupted due to another encounter in the cluster core ([Antonini et al. 2016](#)). Mergers from Lidov-Kozai oscillations in triples will likely imprint a unique eccentricity distribution relative to other in-cluster mergers. This amplification will be investigated further in future work.

#### 4.3. *Effect of cluster properties on highly-eccentric GW inspirals*

Though the detailed cluster properties do not affect the relative fraction of eccentric inspirals between binary-binary and binary-single encounters, the inspiral cross-section and probability are sensitive to the cluster property particulars. As anticipated in [Samsing \(2018\)](#), we find the cluster compactness primarily influences the inspiral probability in a given cluster. As cluster cores become more compact, the escape velocity necessary to eject binaries from strong encounters will increase, which leads to binaries achieving harder orbits before it is energetically probable for them to be ejected. We find that the inspiral probability for a BH encounter scales linearly with the cluster compactness for lower values of  $M/R$ , in both the binary-binary and binary-single cases. However, as can be seen in Figure 4, though the inspiral probability continues to monotonically increase it begins to flatten as we push to the most compact cluster models. This may be a consequence of massive clusters with dense cores also having significantly higher velocity dispersions,

increasing the chance of ionizing encounters and short-lived RIs.

The inspiral probability from binary-binary encounters in the clusters we examine range from  $\sim 0.002$ – $0.02$ . Therefore, in our most optimistic models a binary-binary BH encounter will lead to an eccentric GW capture approximately once every 50 binary-binary encounters. However, massive and compact clusters are highly efficient at ejecting their black holes (Chatterjee et al. 2016). In the local universe, black holes are more likely to reside in the cores of more diffuse clusters, where an appreciable number of black holes may still be retained in the segregated cluster core. Therefore, the models with lower compactness are more representative of the BH population in the local universe, and RI inspirals are more likely to occur once every  $\sim 300$ – $500$  binary-binary encounters.

#### 4.4. Eccentricity and prospects of measurability

BBH inspirals assembled through dynamical encounters imprint unique features in their eccentricity distributions, which may be a key driver in disentangling the relative rates of various proposed BBH formation scenarios. Population modeling predicts highly overlapping distributions of masses which may prove very difficult to leverage in attempts to disentangle formation channels (e.g., Zevin et al. 2017), and if natal spins of heavy stellar mass black holes are naturally low as current BBH detections may indicate, the majority of GW spin measurements may also prove uninformative (Farr et al. 2017a,b).

In the context of current ground-based GW detectors, GW captures in GC cores are a promising scenario for detectable eccentricity, as the Advanced LIGO/Virgo network will be able to distinguish an eccentric from a circular binary in systems similar to GW150914 if the eccentricity is  $\gtrsim 0.05$  (Lower et al. 2018). As seen in Figure 5, the eccentricity distribution of GW captures peaks at approximately 0.05 at a GW frequency of 10 Hz, indicating a substantial fraction of these systems will have discernible eccentricity if they are detected. Furthermore, we see a spike in the eccentricity distribution of GW captures near  $e \approx 1$  from systems which become bound BBHs *inside* the LIGO/Virgo band. However, the detectability and selection biases inherent to such highly-eccentric sources are difficult to ascertain, as substantial eccentricity will also limit the effectiveness of current matched-filtering searches, which search the data using quasi-circular, aligned-spin templates.

Ejected and in-cluster binary inspirals will have eccentricities too low to differentiate between circular signals at a GW frequency of 10 Hz. However, space-based GW detectors such as LISA will be sensitive to orbital frequencies ranging from  $10^{-4}$ – $10^{-1}$  and orbital eccentricities at  $10^{-2}$  and possibly as low as  $10^{-3}$  (Nishizawa et al. 2016; Breivik et al. 2016).

We show the eccentricity distribution of these two populations at  $10^{-2}$  Hz with dashed lines in Figure 5. Similar to the binary-single interactions studied in Samsing & D’Orazio (2018) and D’Orazio & Samsing (2018), we find these populations of BBHs formed through binary-binary encounters to have eccentricities measurable by LISA. Therefore, the combination of ground-based and space-based detectors may be useful in disentangling these three dynamically-induced inspiral scenarios.

We also show inspiral times of the three populations in the right panel of Figure 5. At first glance, the extremely short inspiral timescales of highly-eccentric binaries seems promising; the probability of a detection scales inversely with the delay time as  $1/\tau_{\text{delay}}^4$  if the rate of such interactions is constant throughout the age of the Universe. However, these rapid inspiral timescales may cause the majority of such systems to merge early on in the history of the cluster. If this is the case, BBH mergers from RIs would occur at redshifts of  $z \approx 1$ – $2$ , well beyond the reach of current GW detectors. However, pN cluster modeling has shown that a significant number of BHs are still retained in GC cores at the present day, and inspirals from GW captures still constitute  $\sim 10\%$  of the BH mergers from GCs in the local universe (Rodríguez et al. 2018a).

For the most part, the eccentricity distributions of our GC inspirals are consistent with previous work (cf. Samsing & Ramirez-Ruiz 2017; Rodríguez et al. 2018a). We note that Rodríguez et al. (2018a) reported a slightly different distribution for the IN-CLUSTER BINARY INSPIRAL population; in Figure 5 we do not resolve a peak at an eccentricity of  $10^{-3}$ . This discrepancy is due to a misclassification of triple systems in Rodríguez et al. (2018a) and will be resolved in an upcoming publication (Rodríguez et al. 2018b). We also find that GW captures constitute roughly 17% of all GC inspirals that originate from binary-binary BH interactions. However, this number should be taken with caution, as we do not weight our cluster models by the cluster mass function of the local universe, and a proper local rate estimate will need to convolve the formation time of the different GC inspiral populations with their respective delay time distribution.

Since the scattering experiments performed in this study only record the orbital properties of inspiraling binaries once the simulations terminate, the inspiral times of GW captures from the formation of the IMS binary synthesized during RI are approximated by assuming all systems are formed at a reference eccentricity of  $(1 - e_{\text{ref}}) = 10^{-3}$  (see Section 3.2.2). In the high-eccentricity limit, the inspiral time goes as

$$\tau_{\text{insp}}(a_0, e_0) \propto a_0^4 (1 - e_0)^{7/2} \simeq \frac{1}{\sqrt{1 - e_0^2}}, \quad (1 - e_0^2 \ll 1) \quad (23)$$

This approximation is supported by the continuous distribution found between the GW CAPTURE and IN-CLUSTER

BINARY INSPIRAL populations in the right panel of Figure 5, where the orbital properties for the latter population are recorded post-interaction and inspiral times calculated in the typical way (Peters 1964). Though inspirals near the LIGO/Virgo band may have formed at eccentricities higher than our reference eccentricity, this approximation only constitutes an estimate of the inspiral time at binary formation and does not affect any of the main results in this study.

Lastly, we find that the eccentricity distributions of BBH mergers from binary-binary and binary-single encounters are virtually identical, indicating that the eccentricities themselves will not help decipher which type of resonant dynamical encounter led to the merger. Furthermore, the mass distributions of BHs involved in GW CAPTURES, IN-CLUSTER BINARY INSPIRALS, and EJECTED INSPIRALS are indistinguishable. However, our scattering experiments weight all interactions over the cluster lifetime equally; properly accounting for cluster evolution and convolving delay times with binary formation times may find distinguishing characteristics in the mass distributions for cluster mergers in the local universe. Accurate measurements of the rate of highly-eccentric BBH mergers from the accumulation of GW detections over next few years will help to establish a rate of these exotic signals and provide further insight into the relative contribution of binary-binary interactions in facilitating GW captures during RIs within GCs. Furthermore, if the rate of GW captures compared to in-cluster binary inspirals proves to be constant across globular clusters, we could leverage the detection of highly-eccentric signals to gain insight into the total rate of BBH mergers from globular clusters.

#### 4.5. Post-Newtonian equations of motion

We find the inclusion of pN terms in  $N$ -body scattering experiments to have a negligible effect on the Newtonian end-states of binary-binary encounters. In the context of GW inspirals, previous studies have already discovered that the energy dissipative 2.5pN term plays an important role in facilitating in-cluster mergers in hardened, eccentric binaries between encounters and in the chaotic RIs themselves. This study was the first to examine the effect of lower-order, non-dissipative 1pN and 2pN terms in the equations of motion used in  $N$ -body scattering experiments. Though the 1pN and 2pN terms do not dissipate orbital energy, these lower-order terms are the primary driver of certain aspect of general relativistic orbital evolution such as periaapse precession and play an important role in the stability of secularly evolving systems such as hierarchical triples (Blaes et al. 2002).

Particularly in the case of 4-body encounters, the inclusion of these terms may have proven important in accurately capturing the probability of GW captures, especially if many inspirals were the result of short-lived hierarchical triples. However, we find that these terms have no noticeable effect

on the probability of GW captures during resonating encounters, implying that using only the 2.5pN term suffices in accurately capturing the probability of inspirals during strong BH encounters in GCs.

Nonetheless, the inspiraling encounters studied are in a highly-relativistic regime; as BBHs approach merger their velocities reach appreciable fractions of the speed of light. Though higher-order pN terms will not affect our probabilistic measurements, truncating the pN expansion may lead to inaccuracies in the integration of the system as it approaches merger, and thereby lead to errors in the measurements of orbital quantities such as the SMA and eccentricity at a particular GW frequency. We therefore stop our integration at a particular threshold value of the SMA, namely when the binary SMA is less than ten times the sum of the two BH Schwarzschild radii (equivalent to  $40M$  in geometrized units, assuming equal masses). Two  $20 M_{\odot}$  BHs on a circular orbit at this SMA would be moving at  $\sim 0.2c$ , meaning the contribution from the 3-pN term is  $\sim 0.2\%$  that of the lowest order pN term. Furthermore, such a system would merge in just a few seconds, making the possibility of perturbations from other components in the encounter negligible. However, terminating the integration at larger SMA values should still suffice; even at an SMA of  $100M$  two  $20 M_{\odot}$  BHs on a circular orbit would merge in less than 100 seconds. In the future, when performing pN  $N$ -body scattering experiments it may therefore be more accurate to halt the  $N$ -body integration at larger orbital separations and evolve the orbital properties of the system forward numerically to the GW frequencies of interest. This can either be accomplished by terminating the simulations once an assigned tidal threshold is surpassed as in Samsing et al. (2014) or by choosing a fixed orbital separation at which to terminate that is large enough such that the Newtonian orbital parameters are still accurate yet small enough so perturbations from other particles in the interaction are negligible for the remainder of the inspiral; this methodology will be explored further in upcoming work (Rodriguez et al. 2018b).

## 5. CONCLUSION

In this study, we systematically investigated the contribution of binary-binary encounters to the population of eccentric BH inspirals in GCs, derived scaling relations for GW inspirals due to binary-binary interactions, quantified the importance of lower-order (non-dissipative) pN terms in facilitating eccentric BBH mergers, and gauged the efficiency and properties of eccentric GW captures from realistic cluster models. Our key findings are:

1. Though less common than binary-single BH interactions in GCs, binary-binary BH interactions are  $\sim 3$ – $4$  times more likely to induce an inspiral during a RI, and therefore contribute to  $\sim 25$ – $45\%$  of the total num-

- ber of GW captures originating from GCs where the remaining are from binary-single interactions.
2. The inspiral probability from binary-binary encounters follows the same SMA and mass scaling relation as binary-single encounters:  $\mathcal{P}_{\text{insp}} \propto (M/a_0)^{5/7}$ .
  3. Inspiral probabilities for both binary-binary and binary-single interactions monotonically increase as a function of the compactness of the cluster environment.
  4. The relative contribution of GW captures induced from binary-binary interactions to the total number of GW captures is insensitive to the properties of the cluster environment.
  5. Non-dissipative pN terms play a negligible effect in inducing inspirals during chaotic BH encounters in GCs; the inspiral cross-section can be accurately captured by only including the Newtonian and 2.5pN terms in the  $N$ -body equations of motion.
  6. BBH eccentricity distributions produced from binary-binary encounters in GCs are similar to those produced from binary-single encounters and lead to three distinct populations of BBH mergers: ejected inspirals, in-cluster binary inspirals, and GW captures. The BBH mergers from each population have a distinct eccentricity distribution. GW captures generally have eccentricities measurable by LIGO/Virgo, whereas in-

cluster binary mergers and ejected mergers have eccentricities measurable by LISA.

7. Eccentric BBH inspirals formed in the cores of GCs occur at rates accessible to the Advanced LIGO/Virgo network. A single observation of such a signal will highly constrain its formation scenario, and a population of such detections could lead to the most stringent constraints on the relative rates of BBH formation channels.

MZ would like to express thanks to Kyle Kremer, Chris Pankow, and Fred Rasio for stimulating discussions and valuable insight into this study, and Christopher Berry for useful comments on this manuscript. This work was initiated and supported by the 2017 Kavli Summer Program in Astrophysics at the Niels Bohr Institute in Copenhagen, and the authors would like to thank DARK at the University of Copenhagen for incredible hospitality. The 2017 Kavli Summer Program program was supported by the the Kavli Foundation, Danish National Research Foundation (DNRF), the Niels Bohr International Academy and DARK. MZ greatly appreciates support from the NSF GK-12 graduate student fellowship, under grant number DGE-1007911. CR acknowledges support from the Pappalardo Fellowship in Physics at MIT. ER thanks the DNRF for support as a Niels Bohr Professor.

## REFERENCES

- Aasi, J., Abbott, B. P., Abbott, R., et al. 2015, *Classical and Quantum Gravity*, 32, [arXiv:1411.4547](#)
- Abadie, J., Abbott, B. P., Abbott, R., et al. 2010, *Classical and Quantum Gravity*, 27, 173001
- Abbott, B. P., Abbott, R., Abbott, T. D., et al. 2016a, *Physical Review X*, 6, 041015
- . 2016b, *Physical Review Letters*, 116, 1
- . 2016c, *Physical Review Letters*, 116, 1
- . 2017a, *Physical Review Letters*, 118, 1
- . 2017b, *The Astrophysical Journal Letters*, 35
- . 2017c, *Physical Review Letters*, 119, 1
- Acernese, F., Agathos, M., Agatsuma, K., et al. 2015, *Classical and Quantum Gravity*, 32, [arXiv:1408.3978](#)
- Antonini, J. M., & Thompson, T. A. 2016, *Monthly Notices of the Royal Astronomical Society*, 456, 4219
- Antonini, F., Chatterjee, S., Rodriguez, C. L., et al. 2016, *The Astrophysical Journal*, 816, 65
- Antonini, F., Murray, N., & Mikkola, S. 2014, *Astrophysical Journal*, 781, [arXiv:arXiv:1308.3674](#)
- Antonini, F., & Perets, H. B. 2012, *Astrophysical Journal*, 757, [arXiv:1203.2938](#)
- Antonini, F., Toonen, S., & Hamers, A. S. 2017, *The Astrophysical Journal*, 841, 77
- Bellazzini, M., Fusi Pecci, F., Messineo, M., Monaco, L., & Rood, R. T. 2002, *Aj*, 123, 1509
- Blaes, O., Lee, M. H., & Socrates, A. 2002, *The Astrophysical Journal*, 578, 775
- Blanchet, L. 2014, Gravitational radiation from post-newtonian sources and inspiralling compact binaries
- Breivik, K., Rodriguez, C. L., Larson, S. L., Kalogera, V., & Rasio, F. A. 2016, *The Astrophysical Journal Letters*, 830, 1
- Chatterjee, S., Fregeau, J. M., Umbreit, S., & Rasio, F. A. 2010, *Astrophysical Journal*, 719, 915
- Chatterjee, S., Rodriguez, C. L., & Rasio, F. A. 2016, *The Astrophysical Journal*, 834, 1
- Coughlin, M., Meyers, P., Thrane, E., Luo, J., & Christensen, N. 2015, *Physical Review D - Particles, Fields, Gravitation and Cosmology*, 91, 1

- D’Orazio, D. J., & Samsing, J. 2018, [arXiv:1804.06519](#)
- Downing, J. M. B., Benacquista, M. J., Giersz, M., & Spurzem, R. 2009, *Monthly Notices of the Royal Astronomical Society*, 1962, 1946
- . 2011, *Monthly Notices of the Royal Astronomical Society*, 147, no
- Farr, B., Holz, D. E., & Farr, W. M. 2017a, *The Astrophysical Journal Letters*, 854, L9
- Farr, W. M., Stevenson, S., Miller, M. C., et al. 2017b, *Nature*, 548, 426
- Fishbach, M., Holz, D. E., & Farr, B. 2017, *The Astrophysical Journal Letters*, 840, L24
- Fregeau, J. M., Cheung, P., Zwart, S. F. P., & Rasio, F. A. 2004, *Monthly Notices of the Royal Astronomical Society*, 352, 1
- Fregeau, J. M., & Rasio, F. A. 2007, *The Astrophysical Journal*, 658, 1047
- Gerosa, D., Berti, E., O’Shaughnessy, R., et al. 2018, 1
- Gondán, L., & Kocsis, B. 2018, [arXiv:arXiv:1809.00672v1](#)
- Gondán, L., Kocsis, B., Raffai, P., & Frei, Z. 2017a, *The Astrophysical Journal*, 855, 34
- . 2017b, *The Astrophysical Journal*, 860, 5
- Gültekin, K., Miller, M. C., & Hamilton, D. P. 2006, *The Astrophysical Journal*, 640, 156
- Hamers, A. S., Bar-Or, B., Petrovich, C., & Antonini, F. 2018, 1, [arXiv:arXiv:1805.10313v2](#)
- Hansen, R. O. 1972, Post-Newtonian gravitational radiation from point masses in a hyperbolic kepler orbit
- Haster, C.-J., Antonini, F., Kalogera, V., & Mandel, I. 2016, *The Astrophysical Journal*, 832, 1
- Heggie, D. C. 1975, *Monthly Notices of the Royal Astronomical Society*, 173, 729
- Hoang, B.-m., Naoz, S., Kocsis, B., Rasio, F. A., & Dosopoulou, F. 2017, *The Astrophysical Journal*, 856, 140
- Huerta, E. A., Kumar, P., Agarwal, B., et al. 2017, *Physical Review D*, 95, 1
- Huerta, E. A., Moore, C. J., Kumar, P., et al. 2018, *Physical Review D*, 97, 24031
- Hut, P., & Bahcall, J. N. 1983, *The Astrophysical Journal*, 268, 319
- Hut, P., McMillan, S., Goodman, J., et al. 1992, *Publications of the Astronomical Society of the Pacific*, 104, 981
- Ivanova, N., Belczynski, K., Fregeau, J. M., & Rasio, F. A. 2005, *Monthly Notices of the Royal Astronomical Society*, 358, 572
- Joshi, K. J., Rasio, F. A., & Portegies Zwart, S. P. 2000, *ApJ*, 540, 969
- Klein, A., Boetzel, Y., Gopakumar, A., Jetzer, P., & de Vittori, L. 2018, [arXiv:1801.08542](#)
- Kocsis, B., & Levin, J. 2012, *Physical Review D - Particles, Fields, Gravitation and Cosmology*, 85, 1
- Lee, W. H., Ramirez-Ruiz, E., & De Van Ven, G. 2010, *Astrophysical Journal*, 720, 953
- Leigh, N. W., Stone, N. C., Geller, A. M., et al. 2016, *Monthly Notices of the Royal Astronomical Society*, 463, 3311
- Leigh, N. W. C., Geller, A. M., Shara, M. M., et al. 2017, *Monthly Notices of the Royal Astronomical Society*, 471, 1830
- Lightman, A. P., & Shapiro, S. L. 1978, *Reviews of Modern Physics*, 50, 437
- Liu, B., & Lai, D. 2018, 11, 1
- Lower, M. E., Thrane, E., Lasky, P. D., & Smith, R. 2018, 1
- Mandel, I., Farr, W. M., Colonna, A., et al. 2016, *Monthly Notices of the Royal Astronomical Society*, 7, 1
- Mardling, R. A., & Aarseth, S. J. 2001, *Monthly Notices of the Royal Astronomical Society*, 321, 398
- McMillan, S., Hut, P., & Makino, J. 1991, *The Astrophysical Journal*, 111
- Messick, C., Blackburn, K., Brady, P., et al. 2017, *Physical Review D*, 95, 1
- Mora, T., & Will, C. M. 2004, *Physical Review D - Particles, Fields, Gravitation and Cosmology*, 69, [arXiv:0312082 \[gr-qc\]](#)
- Morscher, M., Umbreit, S., Farr, W. M., & Rasio, F. A. 2013, *Astrophysical Journal Letters*, 763, 2006
- Nishizawa, A., Berti, E., Klein, A., & Sesana, A. 2016, *Physical Review D*, 94, 1
- O’leary, R. M., Kocsis, B., & Loeb, A. 2009, *Monthly Notices of the Royal Astronomical Society*, 395, 2127
- O’Leary, R. M., Meiron, Y., & Kocsis, B. 2016, *The Astrophysical Journal*, 824, L12
- Peters, P. C. 1964, Gravitational Radiation and the Motion of Two Point Masses
- Portegies Zwart, S. F., & McMillan, S. L. W. 2000, *The Astrophysical Journal Letters*, 528, 17
- Quinlan, G. D., & Shapiro, S. L. 1987, *The Astrophysical Journal*, 321, 199
- Randall, L., & Xianyu, Z.-z. 2018a, *The Astrophysical Journal*, 864, 134
- . 2018b, *The Astrophysical Journal*, 853, 93
- Rebei, A., Huerta, E. A., Wang, S., et al. 2018, 1
- Rodriguez, C. L., Amaro-Seoane, P., Chatterjee, S., & Rasio, F. A. 2018a, *Physical Review Letters*, 120, 151101
- Rodriguez, C. L., Amaro-Seoane, P., Zevin, M., et al. 2018b, in prep.
- Rodriguez, C. L., & Antonini, F. 2018, 1
- Rodriguez, C. L., Chatterjee, S., & Rasio, F. A. 2016a, *Physical Review D*, 93, 1
- Rodriguez, C. L., & Loeb, A. 2018, 1
- Rodriguez, C. L., Morscher, M., Pattabiraman, B., et al. 2015, *Physical Review Letters*, 115, 1
- Rodriguez, C. L., Zevin, M., Pankow, C., Kalogera, V., & Rasio, F. A. 2016b, *The Astrophysical Journal Letters*, 832, 1
- Rubenstein, E. P., & Bailyn, C. D. 1997, *The Astrophysical Journal*, 474, 701



- Samsing, J. 2018, *Physical Review D*, 97, 103014
- Samsing, J., Askar, A., & Giersz, M. 2018, *Astrophysical Journal*, 855, 124
- Samsing, J., & D’Orazio, D. J. 2018, 6, 1
- Samsing, J., & Ilan, T. 2018, *Monthly Notices of the Royal Astronomical Society*, 476, 1548
- Samsing, J., MacLeod, M., & Ramirez-Ruiz, E. 2014, *The Astrophysical Journal*, 784, 71
- . 2017a, *The Astrophysical Journal*, 853, 140
- . 2017b, *The Astrophysical Journal*, 846, 36
- Samsing, J., & Ramirez-Ruiz, E. 2017, *The Astrophysical Journal Letters*, 840, L14
- Schröder, S. L., Batta, A., & Ramirez-Ruiz, E. 2018, *The Astrophysical Journal Letters*, 862, L3
- Sedda, M. A., & Benacquista, M. 2018, [arXiv:1806.01285](https://arxiv.org/abs/1806.01285)
- Silsbee, K., & Tremaine, S. 2017, *The Astrophysical Journal*, 836, 1
- Stevenson, S., Berry, C. P. L., & Mandel, I. 2017, *Monthly Notices of the Royal Astronomical Society*, 2811, 2801
- Stevenson, S., Ohme, F., & Fairhurst, S. 2015, *Astrophysical Journal*, 810, 58
- Tai, K. S., McWilliams, S. T., & Pretorius, F. 2014, *Physical Review D - Particles, Fields, Gravitation and Cosmology*, 90, 1
- Talbot, C., & Thrane, E. 2017, *Physical Review D*, 96, 1
- Tiwari, V., Klimentenko, S., Christensen, N., et al. 2016, *Physical Review D*, 93, 1
- Usman, S. A., Nitz, A. H., Harry, I. W., et al. 2016, *Classical and Quantum Gravity*
- Vitale, S., Lynch, R., Sturani, R., & Graff, P. 2017, *Classical and Quantum Gravity*, 34, 1
- Wen, L. 2003, *The Astrophysical Journal*, 598, 419
- Zevin, M., Pankow, C., Rodriguez, C. L., et al. 2017, *The Astrophysical Journal*, 846, 82